Corrosion Science 108 (2016) 1–10

Contents lists available at ScienceDirect

Corrosion Science

journal homepage: www.elsevier.com/locate/corsci

Anodic characteristics and stress corrosion cracking behavior of nickel rich alloys in bicarbonate and buffer solutions

Natalia S. Zadorozne[a,b,c,*], Mabel C. Giordano[b,d], Alicia E. Ares[a,c], Ricardo M. Carranza[b,d], Raul B. Rebak[e]

[a] Instituto de Materiales de Misiones—IMAM (Consejo Nacional de Investigaciones Científicas y Técnicas—CONICET/Universidad Nacional de Misiones—UNaM), Félix de Azara 1552, 3300 Posadas, Misiones, Argentina
[b] Instituto Sabato—UNSAM/CNEA, Av. General Paz 1499, B1650KNA San Martín, Buenos Aires, Argentina
[c] Facultad de Ciencias Exactas, Químicas y Naturales—FCEQyN/Universidad Nacional de Misiones—UNaM, Félix de Azara 1552, N3300LQD Posadas, Misiones, Argentina
[d] Gerencia Materiales, CNEA, Av. General Paz 1499, B1650KNA San Martín, Buenos Aires, Argentina
[e] GE Global Research, 1 Research Circle, CEB2551, Schenectady, NY 12309, USA

ARTICLE INFO

Article history:
Received 28 September 2015
Received in revised form 22 February 2016
Accepted 24 February 2016
Available online 27 February 2016

Keywords:
Nickel
Polarization
Stress corrosion

ABSTRACT

The aim of this work is to investigate which alloying element in C-22 is responsible for the cracking susceptibility of the alloy in bicarbonate and two buffer solutions (tungstate and borate). Six nickel based alloys, with different amount of chromium (Cr) and molybdenum (Mo) were tested using electrochemical methods and slow strain rate tests (SSRT) at 90 °C. All Cr containing alloys had transgranular cracking at high anodic potential; however, C-22 containing high Cr and high Mo was the most susceptible alloy to cracking. Bicarbonate was the most aggressive of three tested environments of similar pH.

1. Introduction

Nickel can dissolve a large amount of alloying elements while still maintaining its austenitic microstructure, which gives them good ductility and formability behavior at ambient temperatures. There are several groups or families of nickel alloys depending of the alloying elements they contain [1,2]. The family of the Nickel-Chromium-Molybdenum alloys is highly versatile regarding its applications since: it is resistant to both cracking in chloride solutions and localized corrosion such as pitting and crevice corrosion, it remains passive in oxidizing acids (because of Cr), and it has a low corrosion rate in reducing acids (because of the Mo) [3–6]. Hastelloy C-22 (N06022), which belongs to the family of Ni-Cr-Mo alloys, was designed to offer a balanced resistance to corrosion in most industrial environments, including reducing and oxidizing acids [7].

Because of its excellent corrosion resistance, Hastelloy C-22 was selected in 1998 by the US Department of Energy for the fabrication of the external layer of the high level nuclear waste container for the Yucca Mountain permanent repository [8,9]. As a result, a comprehensive testing program was undertaken to characterize the behavior of C-22 under a myriad of conditions. For example, the resistance to general corrosion, localized corrosion and stress corrosion cracking (SCC) were fully investigated in numerous environmental conditions including electrolyte composition, temperature and applied potential [10]. On the stress corrosion cracking side, it was reported that alloy C-22 was resistant to cracking in concentrated chloride solutions up to the boiling point [11]. However, C-22 was reported to undergo SCC using the slow strain rate technique (SSRT) (ASTM G129) in bicarbonate containing electrolytes at temperatures higher than 60 °C, at highly anodic applied potentials, which may not be relevant for the repository site conditions [11–26]. These studies also suggest that the coexistence of HCO_3^- and Cl^- ions is particularly damaging to the resistance of alloy C-22 to SCC. Pure HCO_3^- solutions would cause SCC, but the susceptibility appears to increase with increasing Cl^- concentration in the presence of HCO_3^- [11–26].

It was found experimentally that SCC will occur in a pH range between 8.5 and 10.5. It has been suggested that the susceptibility to SCC (e.g. applied potential, temperature and pH of the solution)

* Corresponding author at: Instituto de Materiales de Misiones—IMAM (Consejo Nacional de Investigaciones Científicas y Técnicas—CONICET/Universidad Nacional de Misiones—UNaM), Félix de Azara 1552, 3300 Posadas, Misiones, Argentina.
E-mail address: nataliazadorozne@gmail.com (N.S. Zadorozne).

http://dx.doi.org/10.1016/j.corsci.2016.02.038
0010-938X/

TABLE 1
Actual composition of the studied nickel alloys.

Actual Composition (wt%)	Alloy					
	C-22	600	800H	201	B-3	Ni-20Cr
Ni	56.58	73.44	31.49	99.50	68.8	79.3
Cr	22.26	16.56	20.92	–	1.17	20.3
Mo	13.90	–	–	–	28.6	0.0004
W	3.15	–	–	–	0.0145	–
Fe	3.81	8.83	44.89	0.11	1.68	0.0255
Si	0.02	0.27	0.28	0.10	0.014	0.0037
Mn	0.24	0.24	1.03	0.23	0.37	0.0006
C	0.004	0.06	0.09	0.02	0.0015	0.002
Other	0.2Co	0.253Al	0.49Al 0.57Ti	0.03Co	0.16Al	0.011Cu
Equivalent weight	23.27	26.50	25.72	29.61	23.49	25.81
Density (g/cm^3)	8.6	8.47	7.95	8.89	9.20	8.44

could be related to the occurrence of an anodic peak in the anodic polarization curves in these media [11,23].

In a previous work, Zadorozne et al. attempted to correlate the SCC susceptibility of nickel (Ni)-based alloys with the presence of an anodic peak in bicarbonate and chloride solutions at 90 °C [9]. They found that all the alloys having an anodic peak in the anodic polarization tests suffered SCC when slowly strained at potentials where the peak appeared [24]. Therefore, the presence of SCC in Alloy C-22 could be associated with the presence of the peak, and both (the peak and SCC) could be linked to the presence of Cr in the alloy [24].

Recently, Mishra et al. observed an anodic peak in chloride solutions containing bicarbonate for Hybrid BC-1 (a Ni-Cr-Mo alloy). They demonstrated using X-ray photoelectron spectroscopy (XPS) analyses that, at a lower potential, prior to the current increase, the surface was covered by a thin oxide with high Cr (III) oxide (Cr_2O_3) content and containing Mo in several oxidation states [25,26]. Mishra et al. also showed that a pH > 8.6 is required for the anodic peak to appear in various commercially available Ni–Cr–Mo (W) alloys in different buffer solutions, like bicarbonate/carbonate and borates [25,26]. It was also noticed that the apparent breakdown potential (when no peak was observed) and the anodic peak potential were independent of the concentration of Ni, Cr, Mo, W and other minor alloying elements [25,26].

It is important to investigate which alloying element in C-22 is responsible for the cracking susceptibility of the alloy in bicarbonate containing solutions. Six nickel based alloys with different amount of Cr and Mo (among other elements) were selected for the electrochemical tests and response to SSRT. Tests were conducted in several environments with pH > 8.5 at 90 °C. The alloys studied were: (1) C-22, (2) 600, (3) 800H, (4) Ni-20Cr, (5) B-3 (Ni-Mo) and (6) 201 (99.5% Ni).

2. Experimental procedures

2.1. Electrode and solution preparation

The specimens for the electrochemical and SCC tests were machined from mill annealed 1 in (2.54 cm) diameter commercial bar stock wrought alloys (Figs. 1 and 2). The chemical composition of the materials used in this study is provided in Table 1.

The specimens for the electrochemical anodic behavior were parallelepipeds with approximate dimensions of 12 × 12 × 15 mm, a variation of the ASTM G5 [27] specimen (Fig. 1). The exposed area of the specimen to the solution was approximately 10 cm^2. The specimens had a finish grinding of abrasive silicon carbide (SiC) paper #600, and were degreased in acetone and washed in distilled water within the hour prior to testing. All the electrochemical tests were conducted in a 1 L three-electrode glass vessel. Nitrogen (N_2) was purged through the solution 1 h prior to testing and was continued throughout the entire electrochemical polarization test. A water-cooled condenser combined with a water trap was used to avoid evaporation of the solution and to prevent the ingress of air (oxygen) to the test cell. The temperature of the solution was controlled by immersing the cell in a water bath, which was kept at a constant temperature. The reference electrode was a saturated calomel electrode (SCE), which has a potential of 0.242 V more positive than the standard hydrogen electrode (SHE). The reference electrode was connected to the solution through a water-cooled Luggin probe; the reference electrode was kept at room temperature outside of the cell. The electrode potentials were not corrected for the thermal liquid junction potential because it was assumed to be on the order of a few millivolts [28]. The counter-electrode consisted of a flag of platinum (Pt) foil (total area 50 cm^2) spot-welded to a platinum wire. All the potentials in this paper are reported

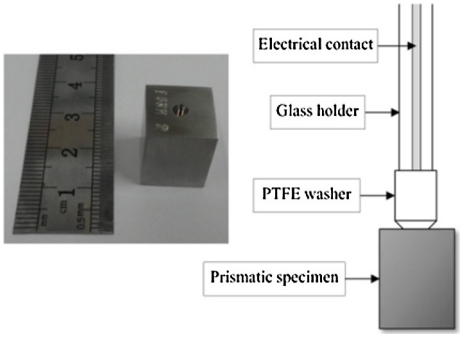

Fig. 1. Image and sketch of prismatic specimens used for polarization studies.

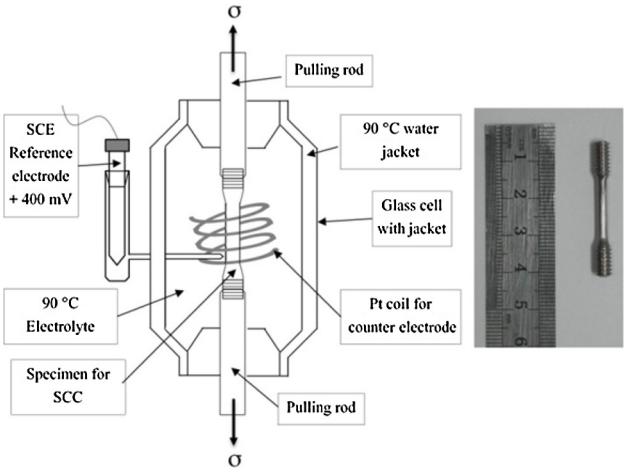

Fig. 2. Specimen used for straining tests. Sketch of glass cell used for SSRT under controlled temperature and potential.

in the SCE scale. The SSRT specimens of C-22, 600, 800H, B-3 and 201 alloys were cylindrical, approximately 180 mm in length and 2.9 mm diameter at the gage (Fig. 2). In the case of the Ni-20Cr alloy, a wire of 1.6 mm diameter was used as the tensile specimen. Before starting the tests, the specimens were longitudinally abraded with #600 abrasive papers, degreased in acetone and rinsed in distilled water.

The SSRT tests were conducted under two conditions: (1) Air at ambient temperature as a control test, and (2) In the studied electrolyte at a constant applied potential of +400 mV SCE to evaluate their susceptibility to SCC. For the SSRT in the electrolyte, a three-electrode electrochemical glass cell was used (Fig. 2). For the SSRT test the temperature of the electrolyte was kept constant by circulating 90 °C water through the glass cell jacket. Both the electrochemical and SSRT tests were performed in: (1) 1.1 mol/L $NaHCO_3$ solution ($8 < pH < 10$), (2) 0.5 mol/L $Na_2WO_4{\cdot}2H_2O$ solution (pH: 9.5), and (3) 0.05 mol/L $Na_2B_4O_7.10H_2O$ solution (pH: 10).

It has been previously reported [10,11] that the presence of an anodic peak in the polarization curves of the Ni-Cr-Mo alloys was independent of the concentration of Ni, Cr, Mo, W and other minor alloying elements. At the same time it has been reported that the anodic peak was present only in electrolytes with higher pH values ($pH > 9$) [25,26]. Taking into account the literature observations [25,26], the current tests were conducted in two media with pH above and near 9 (borate and tungstate), where the anodic peak in the polarization curves becomes discernible.

The pH of each solution was measured before and after the experiments at room temperature. Post-test examination of the specimens was performed using optical and scanning electron microscopy (SEM).

2.2. Anodic behavior

Before the electrochemical tests, the specimens received a cathodic galvanostatic pretreatment of 50 $\mu A/cm^2$ for 5 min. Then the electrochemical anodic response of the alloys in the electrolytes was evaluated using potentiodynamic polarization tests at a scan rate of 0.167 mV/s. The anodic scan was terminated when the current density reached 3 mA/cm^2.

2.3. Susceptibility to SCC using SSRT

The SSRT technique was used in accordance with the ASTM G129 standard practice [29]. The initial strain rate used in the tensile tests was $1.6 \times 10^{-6}\ s^{-1}$. A potentiostat was used to keep the applied potential constant throughout the test at + 400 mV SCE. The temperature was 90 °C.

3. Results

3.1. Corrosion potential and corrosion rate

Figs. 3 and 4 show the values of the corrosion potential and the corrosion rate respectively, for the six tested alloys in the three deaerated tested electrolytes. The corrosion potential values were taken from the anodic polarization curves when the net circulating current was zero. The values of corrosion potential are for short immersion times and may not represent the values for longer immersion or in aerated electrolytes. The corrosion rates (also listed in Table 2) were calculated from the anodic polarization using Tafel slopes and the Faraday second law to convert corrosion current into corrosion rates with the densities and equivalent weights listed in Table 1 [ASTM G 102]. In all the calculations the Tafel constants were assumed to be ±0.120 V/decade. These values of Tafel slopes do not imply the postulation of any corrosion mechanism, they are just the most common values used in literature [30]. The corrosion rates are instantaneous values for short immersion times and used here for comparative purposes only. These corrosion rates may not represent the behavior of the materials for longer immersion times or in aerated electrolytes. Figs. 3 and 4 show that, in general, the lowest corrosion potential for the six alloys was obtained in the bicarbonate solution and the highest corrosion potential corresponded to the borate solution. Some of the lowest corrosion potentials (Fig. 3) were displayed by the alloys B-3 (1.17% Cr) and Ni-201 (without Cr). Fig. 4 and Table 2 show that some of the highest corrosion rates corresponded to the alloys without chromium, that is, the highest corrosion rates in general were related to the lowest corrosion potentials (Fig. 4 and Table 2). In general all the alloys had a higher corrosion rate in the bicarbonate solution.

3.2. Anodic behavior

The potentiodynamic polarization curves of alloys C-22, 600, 800H, Ni-20Cr, B-3 and 201 in the different media at 90 °C are presented in Figs. 5–7. The parameters obtained from these tests are presented in Table 2. The values of anodic peak potential (E_{PEAK}) and the maximum current density at the peak (I_{PEAK}) are listed in

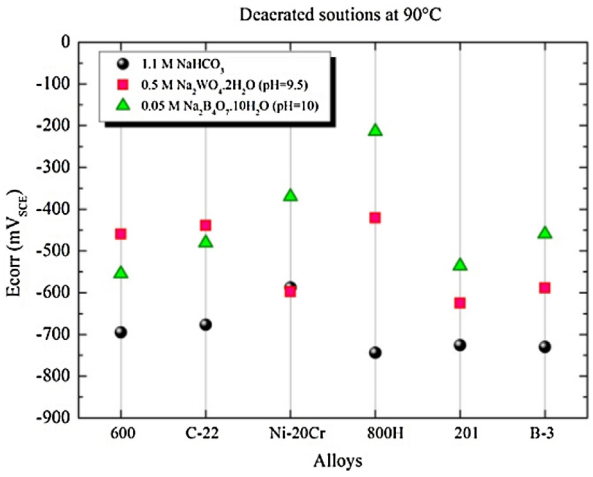

Fig. 3. Corrosion potential of nickel-based alloys in three electrolytes at 90 °C after 30 min immersion in the respective electrolytes. The lowest corrosion potentials are for the bicarbonate solution.

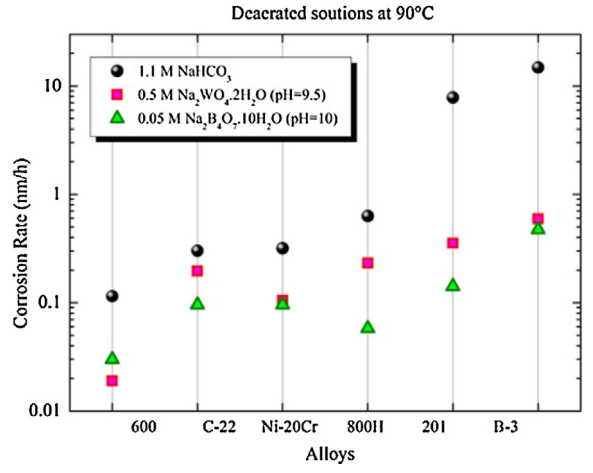

Fig. 4. As immersed instantaneous corrosion rates of nickel-based alloys for three different electrolytes at 90 °C. The highest corrosion rates are for the alloys without significant Cr. The corrosion rates were calculated by converting corrosion current obtained via Tafel slopes and using the Faraday law.

TABLE 2
Data obtained from potentiodynamic polarization curves of alloys C-22, 600, 800H, Ni-20Cr, B-3 and 201 in different media at 90 °C. The corrosion current density was obtained by using Tafel extrapolations from the polarization studies. The Tafel slopes were assumed to be ±120 mV/decade for all the cases. The density and equivalent weights are listed in Table 1. Corrosion rates were calculated using Faraday equation to convert the corrosion current to penetration rates in nanometers per hour.

Alloy	Environment	Ecorr (mV_{SCE})	E_{PEAK} (mV_{SCE})	i_{PEAK} (A/cm^2)	Corrosion Current Density ($\mu A/cm^2$)	Corrosion Rate ($\mu m/y$)	Corrosion Rate (nm/h)
C-22	1.1 mol/L $NaHCO_3$	−677	254	6.24×10^{-4}	0.30	2.64	0.301
	0.5 mol/L $Na_2WO_4 \cdot 2H_2O$	−439	344	6.14×10^{-6}	0.20	1.72	0.196
	0.05 mol/L $Na_2B_4O_7.10H_2O$	−481	292	2.05×10^{-5}	0.10	0.84	0.096
600	1.1 mol/L $NaHCO_3$	−695	293	5.51×10^{-4}	0.10	1.01	0.115
	0.5 mol/L $Na_2WO_4 \cdot 2H_2O$	−460	384	3.90×10^{-6}	0.01	0.17	0.019
	0.05 mol/L $Na_2B_4O_7 \cdot 10H_2O$	−555	313	7.40×10^{-6}	0.02	0.26	0.030
800H	1.1 mol/L $NaHCO_3$	−744	332	2.20×10^{-4}	0.52	5.51	0.629
	0.5 mol/L $Na_2WO_4 \cdot 2H_2O$	−421	425	9.30×10^{-5}	0.19	2.04	0.233
	0.05 mol/L $Na_2B_4O_7 \cdot 10H_2O$	−214	310	7.14×10^{-6}	0.05	0.54	0.062
Ni-20Cr	1.1 mol/L $NaHCO_3$	−588	325	9.80×10^{-4}	0.28	2.78	0.317
	0.5 mol/L $Na_2WO_4 \cdot 2H_2O$	−598	354	6.03×10^{-5}	0.09	0.92	0.105
	0.05 mol/L $Na_2B_4O_7 \cdot 10H_2O$	−370	293	1.07×10^{-5}	0.08	0.84	0.096
B-3	1.1 mol/L $NaHCO_3$	−730	–	- No peak	15.56	129.88	14.826
	0.5 mol/L $Na_2WO_4 \cdot 2H_2O$	−589	–	- No peak	0.62	5.2	0.594
	0.05 mol/L $Na_2B_4O_7 \cdot 10H_2O$	−460	–	- No peak	0.50	4.14	0.473
201	1.1 mol/L $NaHCO_3$	−726	–	- No peak	6.29	68.51	7.821
	0.5 mol/L $Na_2WO_4 \cdot 2H_2O$	−625	–	- No peak	0.29	3.1	0.354
	0.05 mol/L $Na_2B_4O_7 \cdot 10H_2O$	−536	–	- No peak	0.11	1.24	0.142

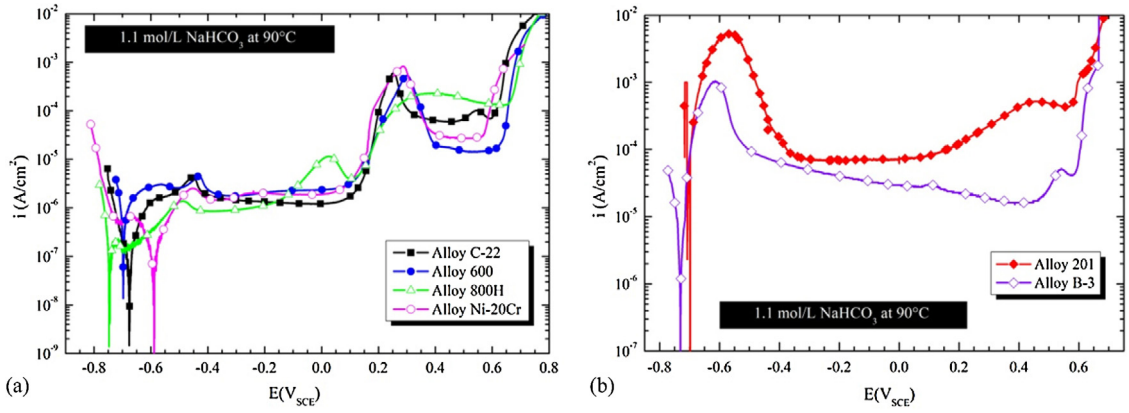

Fig. 5. Potentiodynamic polarization of alloys (a) C-22, 600, 800H, and Ni-20Cr and (b) B-3 and 201 in 1.1 mol/L $NaHCO_3$ at 90 °C.

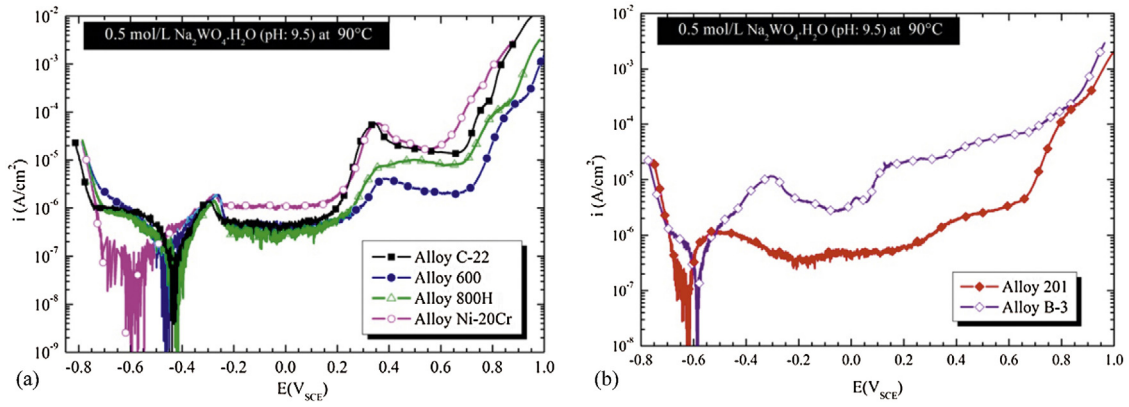

Fig. 6. Potentiodynamic polarization of alloys (a) C-22, 600, 800H, and Ni-20Cr and (b) B-3 and 201 in 0.5 mol/L $Na_2WO_4 \cdot 2H_2O$ (pH 9.5) at 90 °C.

this Table together with Ecorr, the corrosion current, and the corrosion rate (Table 2). The anodic behavior of alloys C-22, 600, 800H, Ni-20Cr, B-3 and 201 in 1.148 mol/L $NaHCO_3$ at 90 °C is shown in Fig. 5(a) and (b). The bicarbonate solution had a pH of 8 at room temperature before starting the polarization experiments in naturally aerated conditions. Once the tests were completed, the pH of the bicarbonate solution was found to increase to 10. For the alloys containing chromium such as Alloy C-22, above Ecorr, the current displayed a passive behavior with current density values in the order of a few $\mu A.cm^{-2}$. After a passive potential range of

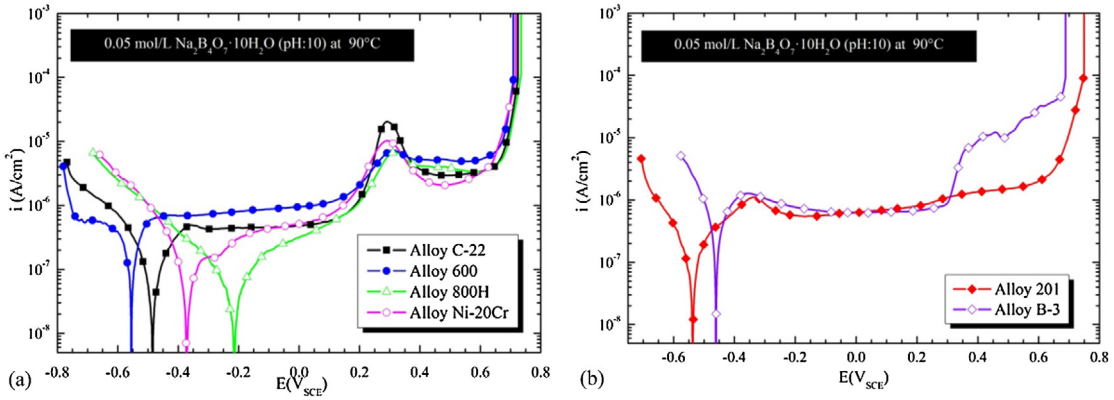

Fig. 7. Potentiodynamic polarization of alloys (a) C-22, 600, 800H, and Ni-20Cr and (b) B-3 and 201 in 0.05 mol/L $Na_2B_4O_7.10H_2O$ (pH 10) at 90 °C.

almost 800 mV (from −600 to +200 mV SCE), the current started to increase at a potential higher than 150 mV SCE (Fig. 5a). The current peaked at approximately 300 mV SCE and then started to decrease. Subsequently the current increased again for potentials higher than 600 mV (Fig. 5a). Even though the current-potential trends of the four alloys (C-22, 600, 800 and Ni-20Cr) were similar, Alloy 800 displayed an additional small current peak at a potential near +20 mV SCE. Alloy 800 also had the lowest decrease in current after the anodic peak in the vicinity of +300 mV. The behavior of 201 (no Cr) and B-3 (1.17% Cr) was different from the other four alloys (Fig. 5b). Both 201 and B-3 showed a large active to passive transition peak and a pseudo passivation current in the potential range from −300 to +600 mV with a current density that was at least one order of magnitude higher than the passive current density observed for the Cr containing alloys (Fig. 5a). Due to the absence of a definite anodic peak for Alloy 201, it was assumed that the anodic peaks in Fig. 5a were associated primarily with one or more of the alloying elements in Alloy C-22. Since alloys without Mo (600 and 800H) also presented the anodic peak, it seems obvious to assume that the anodic peaks in Fig. 5a were produced by the presence of a significant amount of Cr (higher than 15%) in the alloys. This was also confirmed by observing an anodic peak in the Ni-20Cr alloy, while alloy B-3 (1.17% Cr) did not show this peak.

In order to determine whether the presence of the bicarbonate ion was a necessary condition for the formation of the anodic peak in alloy C-22, potentiodynamic anodic polarization tests were performed in other electrolyte media with a pH higher than 9. Results of the anodic potentiodynamic polarization tests in a tungstate solution with pH = 9.5 and in a borate solution with pH = 10 at 90 °C are shown in Figs. 6 ((a), (b)) and 7 ((a), (b)), respectively. The anodic behavior of the six alloys in borate and tungstate electrolytes were in general different from the bicarbonate solution. The corrosion current density of Ni-201 in the potential range from −0.4 V to +0.4 V in tungstate and borate solutions was approximately 2 orders of magnitude lower than in the bicarbonate solution. Also, in the bicarbonate solution Ni-201 had a large anodic peak just above the corrosion potential which was nearly four orders of magnitude higher than in the tungstate and borate solutions. Figs. 5–7 and Table 2 show that all the alloys with anodic peaks in the vicinity of +300 mV SCE had their highest peak current values in the bicarbonate solution. The two alloys with higher iron content (600 and 800H) had the smallest current values at the peaks in the bicarbonate and borate solutions.

3.3. SCC susceptibility

Figs. 8 through 13 show the results of the slow strain rate tests. The stress in Figs. 8 through 13 was calculated using the measured load and the initial cross sectional area of the specimens. Table 3 shows the values of area reduction, rupture times, maximum stress and elongation to rupture in the environment and in air at room temperature (control test). For Alloy C-22, the time to rupture in air was 110 h while in the bicarbonate solution it was only 66 h (Table 3). Observation of the specimens after the tests showed the presence of secondary cracks on the side surface. The tungstate and the borate solutions also induced cracks but the rupture time was longer than in the bicarbonate solution. Alloy C-22

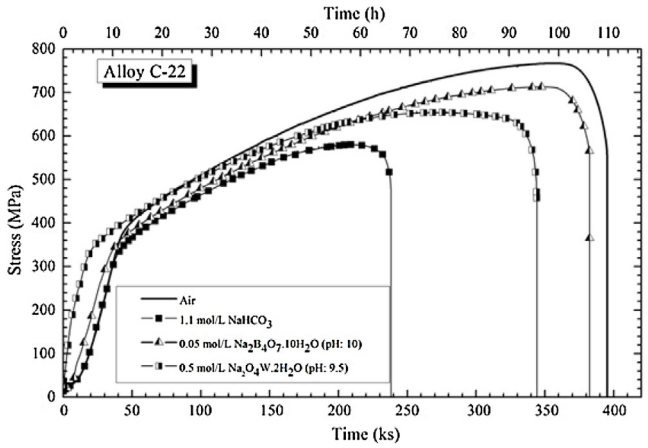

Fig. 8. Stress versus straining time for alloy C-22 in air and in three different solutions at 90 °C and at applied potentials of +400 mV_{SCE}.

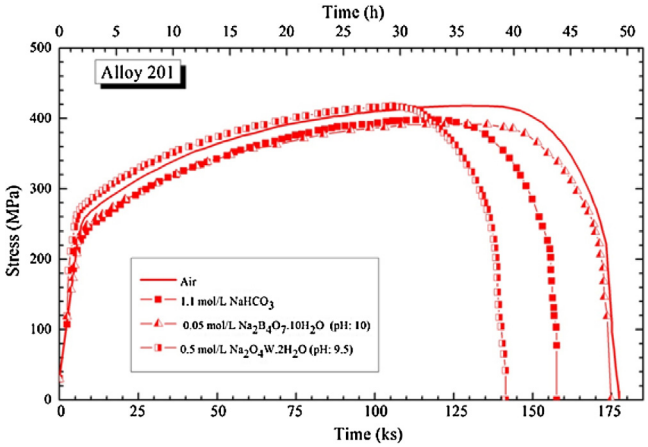

Fig. 9. Stress versus straining time for alloy 201 in air and in three different solutions at 90 °C and at applied potentials of 400 mV_{SCE}.

TABLE 3
SSRT Conditions and Results for Nickel Alloys.

Alloy	Environment Test	Applied Potential mV_{SCE}	Maximum Stress (MPa)	Elongation to Rupture (%)	Reduction of Area (%)	Failure Time (h)	Results
201	Air, RT	–	418.11	39.71	85.48	49	Ductile Failure
	1.1 M $NaHCO_3$	400	398.3	39.24	85.17	44	No SCC
	0.5 M $Na_2WO_4{\cdot}2H_2O$ pH: 9.5		417.67	31.41	88.68	40	No SCC
	0.05 M $Na_2B_4O_7{\cdot}10H_2O$ pH: 10		392.22	37.65	85.76	49	No SCC
800H	Air, RT	–	681.86	40.15	62.88	53	Ductile Failure
	1.1 M $NaHCO_3$	400	516.34	36.9	57.55	47	SCC
	0.5 M $Na_2WO_4{\cdot}2H_2O$ pH: 9.5		537.42	31.20	62.00	45	No SCC
	0.05 M $Na_2B_4O_7{\cdot}10H_2O$ pH: 10		546.53	35.57	63.20	47	No SCC
600	Air, RT	–	733.87	41.35	68.12	67	Ductile Failure
	1.1 M $NaHCO_3$	400	685.20	33.70	47.86	61	SCC
	0.5 M $Na_2WO_4{\cdot}2H_2O$ pH: 9.5		732.10	35.07	57.80	64	No SCC
	0.05 M $Na_2B_4O_7{\cdot}10H_2O$ pH: 10		697.02	37.18	63.27	67	No SCC
B-3	Air, RT	–	838.14	43.95	69.94	60	Ductile Failure
	1.1 M $NaHCO_3$	400	697.26	24.82	42.83	36	SCC
	0.5 M $Na_2WO_4{\cdot}2H_2O$ pH: 9.5		688.75	21.04	51.29	33	SCC
	0.05 M $Na_2B_4O_7{\cdot}10H_2O$ pH: 10		819.71	42.27	70.33	60	No SCC
Ni-20Cr	Air, RT	–	704.99	27.17	71.40	45	Ductile Failure
	1.1 M $NaHCO_3$	400	662.0	21.09	53.70	28	SCC
	0.5 M $Na_2WO_4{\cdot}2H_2O$ pH: 9.5		688.39	21.04	51.29	33	No SCC
	0.05 M $Na_2B_4O_7{\cdot}10H_2O$ pH: 10		708.36	21.05	42.59	33	No SCC
C-22	Air, RT	–	765.79	63.16	68.05	110	Ductile Failure
	1.1 M $NaHCO_3$	400	575.7	37.61	31.83	66	SCC
	0.5 M $Na_2WO_4{\cdot}2H_2O$ pH: 9.5		656.83	57.65	56.32	96	SCC
	0.05 M $Na_2B_4O_7{\cdot}10H_2O$ pH: 10		730.34	40.44	63.60	106	SCC

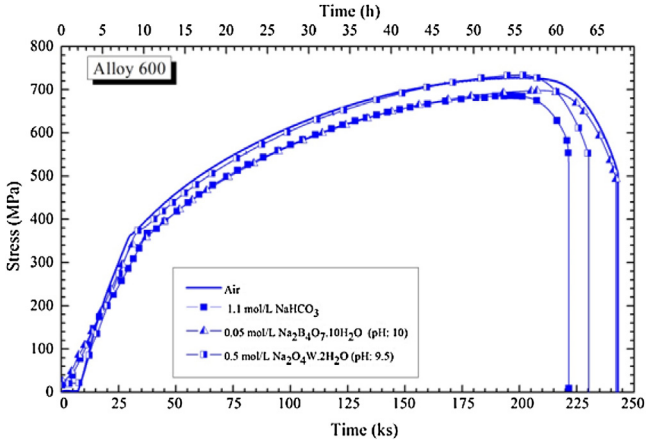

Fig. 10. Stress versus straining time for alloy 600 in air and in three different solutions at 90 °C and at applied potentials of +400 mV_{SCE}.

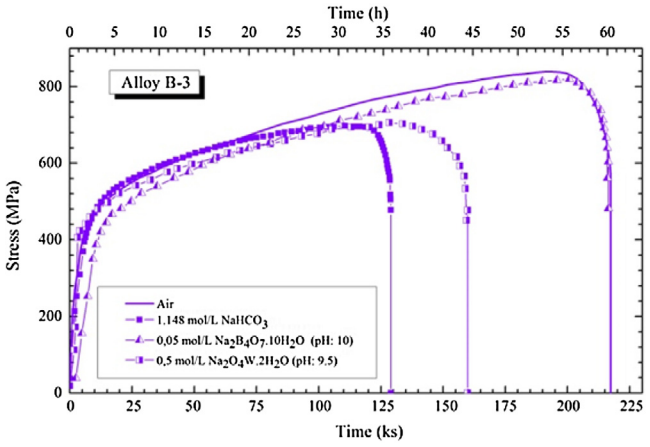

Fig. 12. Stress versus time for alloy B-3 in air and in three different solutions at 90 °C and at applied potentials of +400 mV_{SCE}.

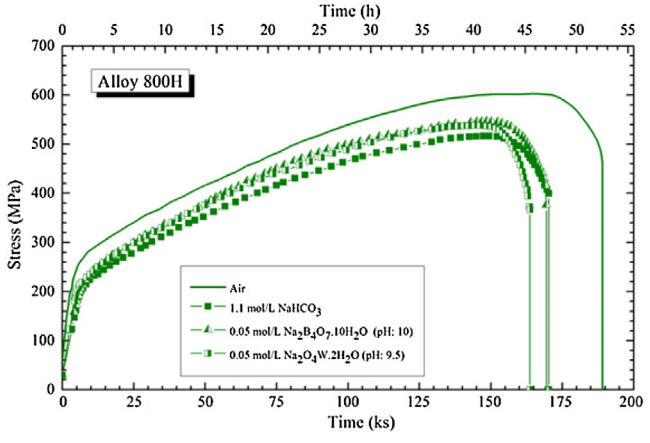

Fig. 11. Stress versus straining time for alloy 800H in air and in three different solutions at 90 °C and at applied potentials of +400 mV_{SCE}.

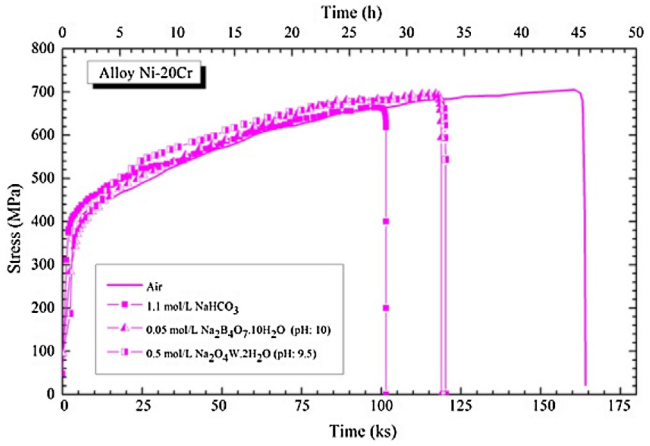

Fig. 13. Stress versus time for alloy Ni-20Cr in air and in three different solutions at 90 °C and at applied potentials of +400 mV_{SCE}.

was the only tested material that exhibited a clear case of SCC in the three tested electrolytes. Other alloys such as 800H, 600, and Ni-20Cr developed clear cases of SCC in the bicarbonate solutions only (Table 3). The results from Table 3 suggest that not only the pH of the solution is the responsible for cracking but the precise composition environment.

To establish whether an alloy was susceptible to SCC, not only the stresses vs. straining times relationships were taken into account but also the observation in the SEM of the tested specimens. If the micrographs did not show evidence of SCC, the specimens were mounted and abraded longitudinally and observed in an optical microscope, in order to determine if the alloy suffered from SCC.

Alloy C-22 showed long cracks when strained in bicarbonate, tungstate and borate solutions at +400 mV SCE (Fig. 14). The stress versus straining time plots for C-22 (Fig. 8) showed a marked decrease both in the maximum load and in the rupture time in the tested electrolytes compared to the test performed in air (Fig. 8).

Stress vs straining time plots of alloy 201 obtained in the different solutions showed a small decrease in the time to failure compared to the control test (Fig. 9 and Table 3). However, no fissures were observed in any of the specimens strained in the electrolytes (Fig. 15). The decrease in testing time in the electrolyte as compared to air could be a consequence of the higher dissolution rates of the Ni-201 materials at the anodic applied potential.

Alloys 600 and 800H showed similar behavior (Figs. 11 and 13). Both Alloys 600 and 800H showed a clear tendency to suffer SCC only in bicarbonate solution (Figs. 16 and 17). The specimens of alloy 600 and 800H were free from cracks when strained in the tungstate and borate solutions. This again speaks of the specific electrolyte solution effect, besides pH.

The specimens of alloy B-3 tested in bicarbonate solution and the tungstate solution (pH: 9.5) showed to be susceptible to SCC (Table 3). While the specimen tested in 0.05 M $Na_2B_4O_7{\cdot}10H_2O$ (pH 10), did not present evidence of SCC (Figs. 12 and 18).

The plots obtained for Ni-20Cr alloy in different media differed from the control test (Fig. 13). However, only the specimen tested in the bicarbonate solution presented SCC. In contrast to all the other alloys studied in this work, Ni-20Cr alloy showed cracks with intergranular morphology, while the others (C-22, 600 and 800H) showed cracks with transgranular morphology (Fig. 19). At this moment it is not clear why Ni-20Cr alloy suffered intergranular cracking while the other alloys suffered transgranular cracking under the tested conditions. This may be a subject of future research.

4. Discussion

Figs. 3 and 4 show the corrosion potential and corrosion rate behavior of the six nickel rich alloys after short term immersion in the deaerated electrolytes. The corrosion potential and corrosion rate (or corrosion current density) (Table 2) are instantaneous values under the short term tested conditions and are not meant to represent the long term behavior of these alloys. It is apparent from Figs. 3 and 4 that the bicarbonate solution offers the lowest corrosion potentials (most active potentials) and the highest corrosion rates. The other two electrolytes (tungstate and borate) offer higher corrosion potentials and lower corrosion rates. For the three tested electrolytes, the highest corrosion rates were for the alloys without Cr, implying that even at the pH values near 9, Cr offers a protective passivation. Interestingly, alloys 600 and 800, which also contain iron (Fe) have some of the lowest corrosion rates. This implies that in the mild alkaline solutions the presence of iron may be beneficial in protecting the alloys against corrosion. That is, iron may partner with Cr to offer a better passivation. A future work may be necessary to actually study the composition of the passive films for these alloys in the tested electrolytes.

Despite the differences in alloying elements, all the Cr containing alloys (C-22, 600, 800 and Ni-20Cr) exhibited a similar polarization behavior. A similar anodic behavior for different commercially available Cr-containing Ni-based alloys has been reported by others. Gruss et al. [30] observed the same type of anodic peak in the polarization tests obtained for the alloy 625 (Ni-21Cr-9Mo) in a solution similar to the one used in the current work. Gruss et al. attributed the anodic peak to the transpassive dissolution of the Cr(III) species, derived from the passive film. That is, after all the Cr(III) in the passive film is oxidized to Cr(VI), the current decreases, forming a peak in the middle of the anodic region. Mishra, et al. [25,26], connected the onset of passive film breakdown to the start of the anodic destruction of the Cr_2O_3 (Cr(III)) barrier layer to yield the more soluble chromate (CrO_4^{2-}) (Cr(VI)).

Mishra et al. [25,26] conducted a series of experiments to determine whether the pH was the critical variable in the anodic process leading to Cr/Mo loss from de passive film. Varying the pH of the solution by adding hydroxide showed that the apparent breakdown/secondary repassivation process (the peak) required an optimum pH of 8.6 for several commercially available Ni-Cr-Mo alloys in different buffer solutions, like bicarbonate/carbonate and borates to generate the peak. That is, the formation of the anodic peak is a consequence of the presence of a passive Cr_2O_3 film on the surface and the formation and stability of this oxide film is highly pH specific.

The potential value at which the anodic peaks appeared shifted only slightly for the three electrolytes. However, the value of the peak maximum current changed significantly for the three tested electrolytes (Figs. 5–7 and Table 2). The fact that the current peak had the highest value for all the alloys in the bicarbonate solution needs to be further studied. This may not be an influence of pH only but also on the nature of the anions present in the electrolyte. Similarly the fact the alloys with iron (600 and 800H) had the lowest current in the peak both for the bicarbonate and borate electrolytes needs to be further investigated. It is likely that Fe and Cr may form a duplex oxide film in the bicarbonate and borate electrolytes offering higher protection of the nickel alloys than with Cr only.

Figs. 6 and 7 also show that Alloy 201 and B-3 did not show a large active to passive transition peak in the tungstate and borate solutions (confirming the higher corrosion rate results for the bicarbonate electrolyte in Fig. 5b). Results show that the presence of bicarbonate ions was not necessary in the electrolyte for Alloy C-22 to exhibit an anodic peak. The anodic peak appeared only when the pH of the electrolyte was maintained in a pH range between 9.5 and 10; however, the characteristics of the peak (such as total charge) maybe dependent on the nature of the anions in the electrolyte (i.e. bicarbonate vs. borate vs. tungstate).

The anodic polarization tests for alloys C-22, 600, 800H, Ni-20Cr, B-3 and 201 reveal that all the alloys that show an anodic peak in the bicarbonate solution, also show the peak in the other electrolyte solutions with pH between 9.5 and 10.

4.1. Correlation between the anodic peak and the susceptibility to cracking

Previous publications linked the SCC susceptibility of alloy C-22 to the presence of an anodic peak during anodic polarization occurring in a range of potentials between +200 and +400 mV_{SCE} in $Cl^- + HCO_3^-$ containing media at temperatures above 60 °C [11–26].

In a recent work, Zadorozne et al. [24] showed that all the alloys having an anodic peak in the anodic polarization tests suffered SCC when strained at potentials where the peak appeared in Cl— and

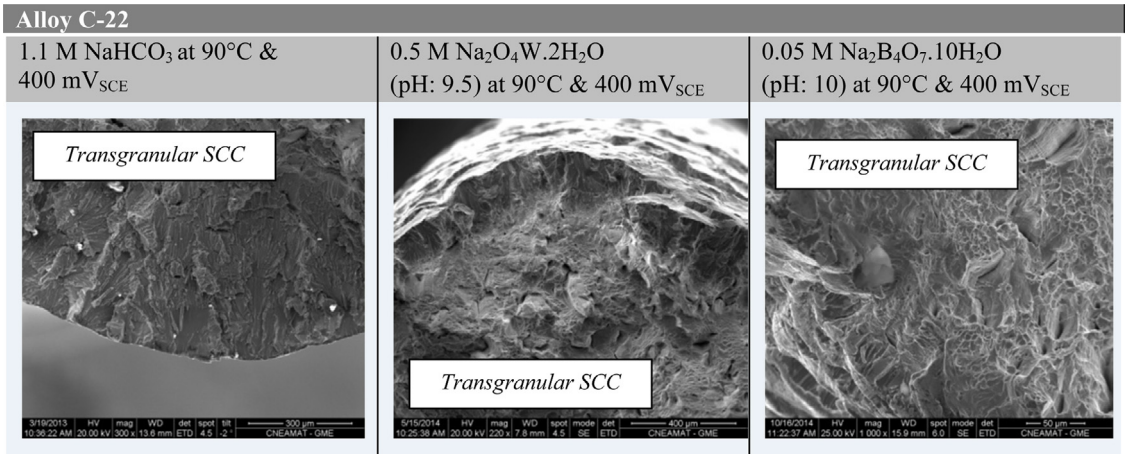

Fig. 14. Macrographs of alloy C-22 fracture surface, after the tensile test in different solutions at 90 °C at 400 mV_{SCE}. SCC is observed in the three tested environments.

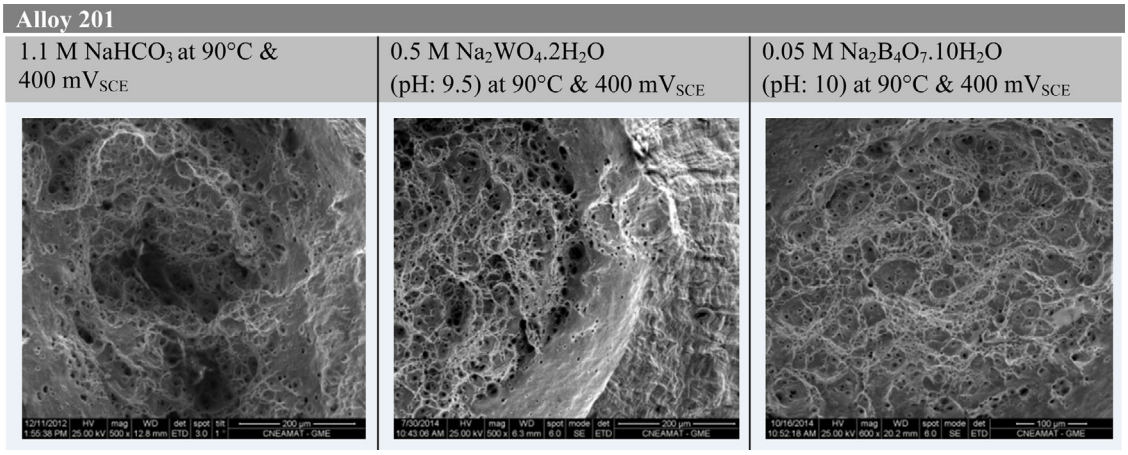

Fig. 15. Macrographs of alloy 201 fracture surfaces, after the tensile test in different solutions at 90 °C at 400 mV_{SCE}. No brittle cracking is observed.

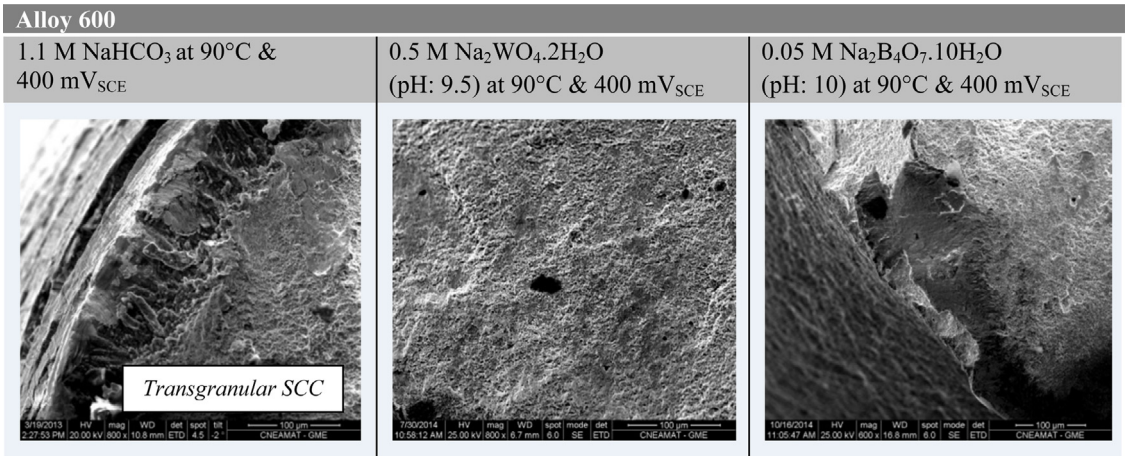

Fig. 16. Macrographs of alloy 600 fracture surface, after the tensile test in different solution at 90 °C and at 400 mV_{SCE}. TG SCC only in the bicarbonate solution.

HCO_3— containing media at 90 °C. They suggested that the presence of SCC in alloy C-22 might be associated with the presence of the peak, and that both (the peak and SCC) might be connected to the presence of Cr in the alloy [24].

The analysis of the results from the current work show that two conditions were necessary for the anodic peak to appear; (1) significant amount of Cr in the alloy, and (2) an electrolyte with a pH between 9.5 and 10. The two materials that did not show the anodic peak were Ni-201 (no Cr) and B-3 (~1%Cr).

All the alloys having an anodic peak in the polarization tests presented cracks during SSRT at applied potentials in the vicinity of the potential of the anodic peak for the bicarbonate solution only. The two other electrolytes (tungstate and borate) also induced the Cr containing alloys to form the peak; however, the alloys did not develop SCC. It is apparent that not only the pH of the electrolyte is

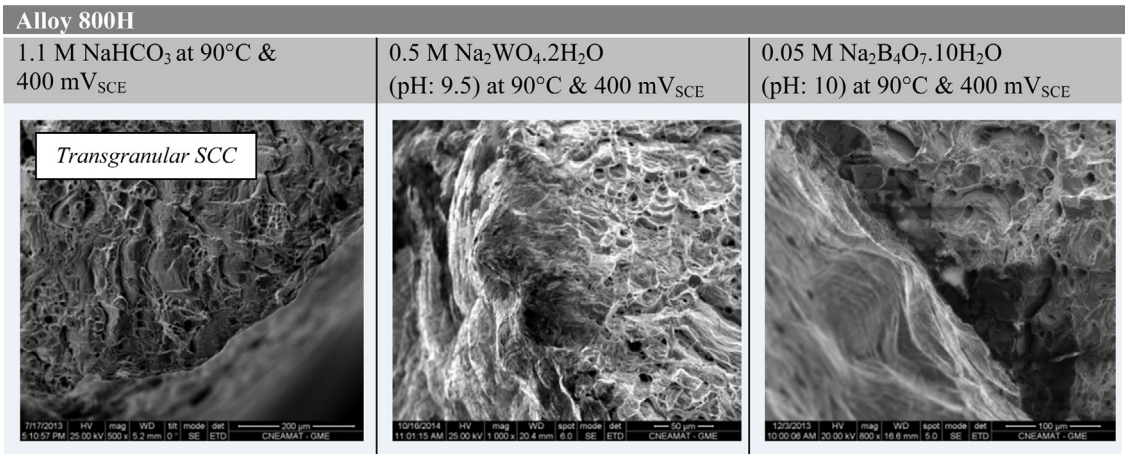

Fig. 17. Macrographs of alloy 800H fracture surface, after the tensile test in different solution at 90 °C and at 400 mV_{SCE}. TG SCC only in the bicarbonate solution.

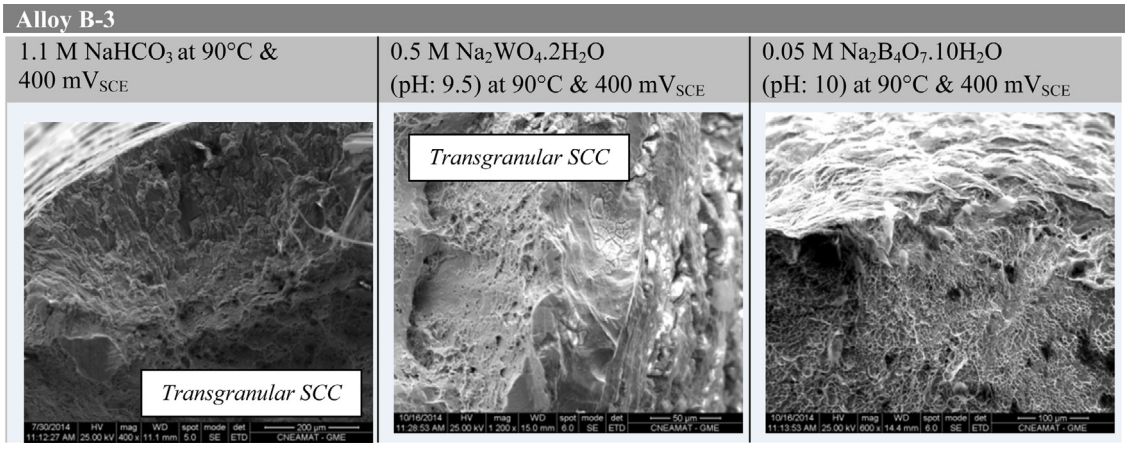

Fig. 18. Macrographs of alloy B-3 fracture surfaces, after the tensile tests in different solution at 90 °C and at 400 mV_{SCE}. TG SCC observed in the bicarbonate and tungstate solutions.

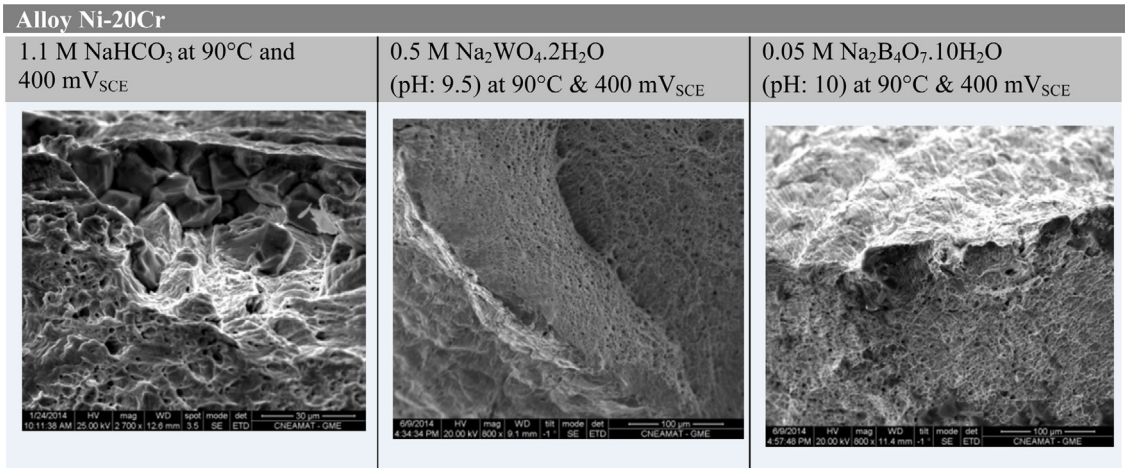

Fig. 19. Macrographs of alloy Ni-20Cr fracture surface, after the tensile tests in different solutions at 90 °C and at 400 mV_{SCE}. IG SCC only in the bicarbonate solution.

important but also the nature of the anion present in the electrolyte. Moreover, the composition of the alloy is significant. Even though all alloys with significant Cr developed cracks in the bicarbonate solution, only C-22 developed cracks in the three electrolytes. In a similar way as stated in previous publications that bicarbonate caused cracking in C-22 and the presence of chloride enhanced this susceptibility, here it can be said that Cr maybe responsible for cracking in the bicarbonate solution but the content of Mo (such as in C-22) enhances the susceptibility of the alloy to cracking.

B-3 also presented SCC under the similar tested conditions even though the low amount of Cr in the alloy may not be significant to contribute to an anodic peak during potentiodynamic polarization. It is not clear at this moment if the small amount of Cr in B-3 may have influenced its susceptibility to cracking.

It appears that SCC of nickel alloys with chromium in the mild environment of electrolytes with a pH above near 9 at 90 °C may be associated to the disruption of the passive film offered by Cr_2O_3. A partial second oxidation of this film to chromate species seems to be the trigger to nucleate cracks during slow strain rate tests. Results also seem to suggest that the presence of Cr + Mo in the alloy makes it more susceptible to cracking since alloys without Mo (such as 800H and 600) do not suffer SCC in tungstate and borate solutions.

Current results show that cracking occurred under dynamic straining conditions (SSRT), that is, it is not known if cracking would also occur under constant load, which could be more representative of an actual industrial application of the chromium containing nickel rich alloys.

5. Conclusions

1 Potentiodynamic polarization tests show that alloys C-22, 800H, 600 and Ni-20Cr presented an anodic peak in a range of potentials between 200 and 400 mV_{SCE} when tested in 1.1 M $NaHCO_3$, 0.5 M $Na_2WO_4.2H_2O$ (pH: 9.5) and 0.05 M $Na_2B_4O_7.10H_2O$ (pH: 10) at 90 °C. This peak was mainly attributed to the presence of Cr in the alloys, and the peak was formed when Cr in the passive film was oxidized from Cr(III) (Cr_2O_3) to Cr(VI) (CrO_4^{2-}).

2 The anodic peak in C-22, 800H, 600, Ni-20Cr appeared when the pH of the electrolyte was in the vicinity of 9. However the size of the peak (total charge) was always the largest in the bicarbonate solution. That is, the peak is not only pH sensitive but the nature of the electrolyte is also important.

3 Specimens of Alloys C-22, 600, Ni-20Cr, 800H and B-3 tested by SSRT in bicarbonate solutions at +400 mV_{SCE} and 90 °C showed SCC. It is apparent that cracking developed at potentials and pH where the passive film is disrupted by a secondary oxidation (Cr(III) to Cr(VI)).

4 C-22 also suffered SCC during SSRT in the borate and tungstate electrolytes at +400 mV SCE and 90 °C. The particular composition of C-22 appears to be the most susceptible to cracking in the tested conditions.

Acknowledgment

Financial support from the Agencia Nacional de Promoción Científica y Tecnológica of the Ministerio de Educación, Ciencia y Tecnología from Argentina is acknowledged.

References

[1] R.B. Rebak, Crystallinne alloys: nickel, in: L.H. Hihara, R.P.I. Adler, R.M. Latanision (Eds.), Environmental Degradation of Advanced and Traditional Engineering Materials, Taylor & Francis Books, Inc., New York, 2013, pp. 197–218.
[2] J.H. Weber, Nickel and nickel alloys: an overview, in: Encyclopedia of Materials: Science and Technology, Elsevier, 2001, pp. 6145–6146.
[3] R.B. Rebak, P. Crook, Nickel alloys for corrosive environments, Adv. Mater. Process. 157 (2000) 37–42.
[4] R.B. Rebak, in: R.W. Cahn, P. Haasen, E.J. Kramer (Eds.), Corrosion and Environmental Degadation in Materials Science and Technology: A Comprehensive Treatment: Corrosion and Environmental Degradation, Volumes I+II, Wiley-VCH Verlag GmbH, Weinheim, Germany, 2000.
[5] R.B. Rebak, Factors affecting the crevice corrosion susceptibility of alloy 22, NACE Corros. 2005 (2005) 1–17 (Pap. 05610).
[6] R.M. Carranza, The crevice corrosion of Alloy 22 in the Yucca Mountain nuclear waste repository, JOM J. Miner. Met. Mater. (2008) 58–65.
[7] Crook Paul, R.B. Rebak, Influence of the environment on the general corrosion rate of alloy 22 (N06022), Transport Store Diposal Radioact. Mater. 483 (2004) 131–136.
[8] G.M. Gordon, Speller Award Lecture: corrosion considerations related to permanent disposal of high-level radioactive waste, Corrosion 58 (2002) 811–825.
[9] O. of C.R.W.M. DOE, Yucca Mountain Science and Engineering Report, DOE/RW-0539, Las Vegas, NV, USA, (2001).
[10] R.B. Rebak, Corrosion testing of nickel and titanium alloys for nuclear waste disposition, Corrosion 65 (2009) 252–271.
[11] K.T. Chiang, D.S. Dunn, G.A. Cragnolino, Effect of simulated groundwater chemistry on stress corrosion cracking of alloy 22, Corrosion 63 (2007) 940–950.
[12] R.B. Rebak, Stress Corrosion Cracking of Nickel Alloys in Stress Corrosion Cracking: Theory and Practice, Woodhead Publishing, Sawston, Cambridge, UK, 2011, pp. 273–306.
[13] J.C. Estill, K.J. King, D.V. Fix, D.G. Spurlock, G.A. Hust, S.R. Gordon, et al., Susceptibility of alloy 22 to environmentally assisted cracking in yucca mountain relevant environments, NACE Corros. 2002 (2002) 1–13 (Pap. 02535).
[14] D.S. Dunn, Y.-M. Pan, G.A. Cragnolino, Stress corrosion cracking of nickel-chromium-molybdenum alloys in chloride solutions, NACE Corros 2002 (2002) 1–20 (Pap. 02425).
[15] P.L. Andresen, P.W. Emigh, L.M. Young, G.M. Gordon, Stress corrosion cracking growth rate behavior of alloy 22 (UNS N06022) in concentrated groundwater, NACE Corros. (2003) 1–31 (Pap. 03683).
[16] D.V. Fix, J.C. Estill, G.A. Hust, L.L. Wong, R.B. Rebak, Environmentally assisted cracking behavior of nickel alloys in simulated acidic and alkaline ground waters using u-bend specimens, NACE Corros. (2004) 1–18 (Pap. 04549).
[17] K.J. King, L.L. Wong, J.C. Estill, R.B. Rebak, Slow strain rate testing of alloy 22 in simulated concentrated ground waters, NACE Corros. 2004 (2004) 1–16 (Pap. 04548).
[18] K.T. Chiang, D.S. Dunn, G.A. Cragnolino, Effect of groundwater chemistry on stress corrosion cracking, NACE Corros. 2005 (2005) (Pap. 05463).
[19] D.S. Chiang, The combined effect of bicarbonate and chloride ions on the stress corrosion cracking susceptibility of alloy 22, NACE Corros 2006 (2006) 1–20 (Pap. 06506).
[20] K.T. Chiang, D.S. Dunn, G.A. Cragnolino, Effect of simulated groundwater chemistry on stress corrosion cracking of alloy 22, Corrosion 63 (2007) 940–950.
[21] D.S. Shukla, Stress corrosion cracking model for alloy 22 in the potential yucca mountain repository environment, NACE Corros. 2006 (2006) 1–25 (Pap. 06502).
[22] D.S. Dunn, K.T. Chiang, G.A. Cragnolino, Surface analysis of alloy 22 under conditions that promote stress corrosion cracking, NACE Corros. (2006) 1–11 (Pap. 06509).
[23] D.V. Fix, J.C. Estill, R.B. Rebak, S.D. Day, K.J. King, G.A. Hust, Influence of environmental variables on the susceptibility of alloy 22 to environmentally assisted cracking, Corrosion 2003 (2003) (Pap 0354).
[24] N.S. Zadorozne, C.M. Giordano, R.B. Rebak, A.E. Ares, R.M. Carranza, Anodic stress corrosion cracking suspectibility of nickel and nickel-Chromium alloys containing molybdenum and iron in bicarbonate plus chloride solutions at 90, Corrosion (2015) 420–432.
[25] A.K. Mishra, S. Ramamurthy, M. Biesinger, D.W. Shoesmith, The activation/depassivation of nickel-chromium-molybdenum alloys in bicarbonate solution: part I, Electrochim. Acta 100 (2013) 118–124.
[26] A.K. Mishra, D.W. Shoesmith, The activation/depassivation of nickel-chromium-molybdenum alloys: an oxyanion or a pH effect—Part II, Electrochim. Acta 102 (2013) 328–335.
[27] ASTM G5-94, Standard reference test method for making potentiostatic and potentiodynamic anodic polarization measurements, in: Annual Book of ASTM Standards, ASTM International, West Conshohocken, PA, 2004, pp. 53–64 (03.02).
[28] A.C. Macdonald, External reference electrodes for use in high temperature aqueous systems, J. Electrochem. Soc. (1979) 6.
[29] ASTM G129, Standard practice for slow strain rate to evaluate the susceptibility of metallic materials to environmentally assisted cracking, in: Annual Book of ASTM Standards, ASTM International, West Conshohocken, PA, 2004, pp. 552–558 (03.02).
[30] K.J. Evans, R.B. Rebak, Corrosion science, a retrospective and current status in honor of Robert P. Frankenthal, Electrochem. Soc. (2002) 344–354.